Cleveland State University
EngagedScholarship@CSU

MSL
ACADEMIC ENDEAVORS

Physics Faculty Publications

Physics Department

12-1-1998

Relaxational Mode Structure for Optical Probe Diffusion in High Molecular Weight Hydroxypropylcellulose

Kiril A. Streletzky
Cleveland State University, K.STRELETZKY@csuohio.edu

George D.J. Phillies
Worcester Polytechnic Institute, phillies@wpi.edu

Follow this and additional works at: https://engagedscholarship.csuohio.edu/sciphysics_facpub

Part of the Physics Commons

How does access to this work benefit you? Let us know!

Publisher's Statement

This is the accepted version of the following article: Kiril A. Streletzky and George D. J. Phillies, "Relaxational mode structure for optical probe diffusion in high molecular weight hydroxypropylcellulose," Journal of Polymer Science Part B: Polymer Physics 36 (17), 3087-3100 (1998). , which has been published in final form at http://onlinelibrary.wiley.com/doi/10.1002/(SICI)1099-0488(199812)36:17%3C3087::AID-POLB9%3E3.0.CO;2-2/pdf

Relaxational Mode Structure for Optical Probe Diffusion in High Molecular Weight Hydroxypropylcellulose

KIRIL A. STRELETZKY, GEORGE D. J. PHILLIES

INTRODUCTION

The mechanism of polymer dynamics in solutions is a major unanswered question that has been studied intensively for many years. There are many different experimental approaches to the problem.[1] One of the widely used techniques is the optical probe diffusion experiment. In this kind of experiment one observes the motion of dilute monodisperse probe particles through the polymer solution of interest. If probes scatter considerably ($\sim$ 99%) more light than the polymer does, then one can obtain crucial information about the polymer dynamics by monitoring the diffusion of probe particles. Optical probe diffusion can be observed by a number of experimental techniques. Our laboratory studies probe diffusion using quasi-elastic light-scattering spectroscopy (QELSS), which infers the dynamic structure factor $S(q, t)$ of the scattered light.

The use of the optical probe technique was pioneered by Turner and Hallett[2] more than 20 years ago. Since then numerous experimental studies in different polymer solutions[3–17] have revealed a wide variety of probe diffusion phenomenologies.

It was demonstrated[18,19] that in systems in which the functional form of $S(q, t)$ is close to a simple exponential one can obtain the probe's self-diffusion coefficient D_p from $S(q, t)$. One can

then compare D_p with the macroscopic zero-shear viscosity η of the solution by using the Stokes–Einstein equation

$$D = \frac{k_B T}{6 \pi \eta R_h} \qquad (1)$$

Here k_B is Boltzmann's constant, T is the absolute temperature, and R_h is the hydrodynamic radius of the diffusing probe. Equation (1) is known to work for mesoscopic probe diffusion in low-viscosity small-molecule solvents. Equation (1) does not always work in high-viscosity large-molecule solvents.[3–6] However, in some systems $S(q, t)$ is highly bimodal, posing the question of how a single diffusion coefficient D_p can represent two decay modes in $S(q, t)$. An alternative detailed lineshape analysis of $S(q, t)$ is needed in this case.

This article addresses the results of a study[20] of probe diffusion in aqueous solutions of hydroxypropylcellulose. The scattering from probes diffusing in this polymer solution reveals a bimodal $S(q, t)$. Lineshape analysis of $S(q, t)$ was employed[20] for this system, finding two distinct modes of the relaxation. An apparent influence of the probe size on the relaxational mode structure was discovered.[20] The detailed lineshape analysis can be found in ref. 20. Here we discuss properties of the spectral parameters that reveal the physical nature of the relaxational mode structure. In our analysis of the physical nature of modes, we also attempted to apply the coupling/scaling model[21] analysis to our system.[22]

The following sections introduce experimental methods, give the important results of ref. 20, present a coupling/scaling model analysis of our data, and discuss the modes' physical interpretations.

EXPERIMENTAL

Quasi-elastic light-scattering spectroscopy studies the temporal evolution of concentration fluctuations in a sample by monitoring the light-scattering intensity $I(q, t)$ (where q is the scattering vector) and calculating the intensity–intensity correlation function:

$$S(q, \tau) = \int_0^T dt I(q, t) I(q, t + \tau). \qquad (2)$$

Here, τ is a shift in time, and T is the duration of the experiment. Our light-scattering spectrometer used a 1.5 W Ar^+ (Spectra-Physics 2020-03) CW laser coupled to a photometergoniometer (Brookhaven Instruments BI-200SM). Sample cells, placed into a decalin-filled index-matching vat, were maintained at 25 ± 0.1°C. Spectra were analyzed with a 270-channel digital multitau correlator (Brookhaven Instruments BI2030AT).

The subject of this study was hydroxypropylcellulose (HPC), nominal molecular weight 1 MDa (Scientific Polymer Products), in aqueous solution. Stock solutions of polymer concentration 7 g/L were prepared in purified water (Millipore Milli-RO, Milli-Q water systems) and diluted to cover polymer concentrations of 0–7 g/L generally at 1 g/L intervals. HPC absorption by probes was prevented by adding a trace amount (based on Phillies et al.[23]) of surfactant [0.2 wt % TX-100 (Aldrich)]. Carboxylate-modified polystyrene latex spheres (PSL) with nominal diameters of 14, 21, 38, 67, 87, 189, 282, and 455 nm (Interfacial Dynamics, Seradyn, Dow Chemicals) were used in the probe diffusion experiments. Because latex spheres are very good scatterers, even trace amounts of PSL (5–10 µL per mL of polymer solution) were enough for probes to dominate the scattering intensity. Probe multiple scattering was avoided by using small probe volume fractions (under 0.001).

The observed spectra in our experiments correspond to probe motion through the practically unseen polymer matrix. There is no sizable contribution from concentration fluctuations of polymer or surfactant. To test this point we directly compared spectra of probe-containing and probe-free polymer solutions under identical operating conditions. Typically $S(q, 0)$ of a probe-free polymer solution is about 1% of $S(q, 0)$ of a probe-containing polymer solution: the probe contribution to the total scattering is far greater than any other contribution. We also subtracted (at the field-correlation function level) spectra of probe-free polymer solutions from spectra of probe-containing polymer solutions to find the contribution of the polymer scattering. The difference spectra then were subjected to our spectral fitting routine, yielding the same fitting parameters (within experimental error) as did unsubtracted probe-containing spectra.

Analyzing our spectra, we found that they were highly bimodal. A calculation of the probe diffusion coefficient D_p from the initial logarithmic slope of $S(q, t)$ therefore does not describe the

long-time part of the spectrum. A systematic analysis of the spectral lineshape is required.

We analyzed the spectral lineshape on the level of field correlation function $g^{(1)}(q, t)$. The intensity–intensity correlation function $g^{(2)}(q, t)$ is related to $g^{(1)}(q, t)$ via

$$g^{(2)}(q, t) = S(q, t) - B = A(g^{(1)}(q, t))^2, \quad (3)$$

where A is the scattering amplitude and B is the baseline, the time-independent part of the spectrum. We tried different forms of $g^{(1)}(q, t)$ to see which one best described $g^{(2)}(q, t)$. We minimized $[g^{(2)}(q, t) - S(q, t)]^2/[S(q, t)]^2$, applying nonlinear least squares and the simplex algorithm.[24]

RESULTS

This section presents a generalized analysis of our light-scattering spectra and physical properties of the modes that were found to compose our spectra. A more detailed description of our findings is found in ref. 20.

Analyzing highly nonexponential $S(q, t)$ of probes of different diameter d we found[20] that probes with $d < 67$ nm clearly have bimodal spectra. Even though spectra of probes with $d \geq 67$ nm do not demonstrate an obvious bimodal lineshape to the eye, they are also found by numerical analysis to be bimodal. The bimodal $g^{(1)}(t)$ that describes our spectra has the form

$$g^{(1)}(t) = (1 - A_f)\exp(-\theta t^\beta) + A_f\exp(-\theta_f t^{\beta_f}). \quad (4)$$

Here, θ, β are the relaxation pseudorate and stretching exponent of the slow mode, θ_f, β_f are the relaxation pseudorate and stretching exponent of the fast mode, and A_f is the amplitude fraction of the fast mode. The visible difference in the lineshape of $S(q, t)$ between small ($d < 67$ nm) and large ($d \geq 67$ nm) probes is reflected in different values of the slow stretching exponent β. For large probes, forcing $\beta \equiv 1$ produced[20] much more stable and reproducible fits then did allowing β to be a free parameter. For small probes, fits with $\beta \approx 0.7$–0.95 gave excellent results.

Our analysis decomposes spectra of polystyrene sphere probes into two modes, a fast stretched-exponential mode and a slower exponential or stretched-exponential mode. It should be emphasized that our interpretation of the modes as stretched exponentials is phenomeno-logical. A group of exponential modes whose sum approximates a stretched exponential decay cannot, within the limits of our experimental method, be distinguished from a single stretched-exponential mode. Our remarks on the properties of single modes may, therefore, actually be statements about the aggregate behavior of a group of modes. However, sums of two pure exponentials do not fit our spectra. A single stretched-exponential mode may be a stretched exponential or an aggregate of pure exponentials, but is observably not a single pure exponential.

Summarizing, in our lineshape analysis we found[20] slightly different but bimodal (fast and slow modes) spectral lineshapes for small and for large probes. Probes with $d < 67$ nm have $g^{(1)}$ in the form of two stretched exponentials, while probes with $d \geq 67$ nm have $g^{(1)}$ in the form of a fast stretched and a slow pure exponential. The difference[20] in the functional description of $g^{(1)}(t)$ between large and small probes remained the same at all polymer concentrations studied. The crossover probe radius separating small and large probe behavior[20] is comparable with the chain dimensions. In particular, small probes are smaller than the hydrodynamic radius of the polymer, while large probes are comparable or larger than the radius of gyration of the polymer. Our spectra thus may be divided naturally by a time scale and probe size into four regimes, namely two modes (fast and slow) for small ($d < R_h$) probes, and two modes for large ($d \geq R_g$) probes.

The difference between large and small probes is made very prominent if one considers the diameter dependence of the pseudorates θ and θ_f. Figure 1(a) gives the probe diameter dependence of θ for each polymer concentration studied. There are two regimes: (1) small probes with no concentration dependence of θ, and (2) large probes with θ strongly depending on c. The transition from small- to large-probe behavior begins as d approaches the hydrodynamic radius R_h of the chain, and is complete for d larger than the radius of gyration R_g of the chain. This length scale remains the same for polymer concentrations up to $c = 7$ g/L, which corresponds to $c[\eta] = 5$. The concentration independence of the transition length scale is inconsistent with some transient gel models. The typical transient gel models[25,26] consider the distance between the chain entanglements ξ as the length scale that influences the probe motion through the polymer. The polymer solution, according to these models, would act like
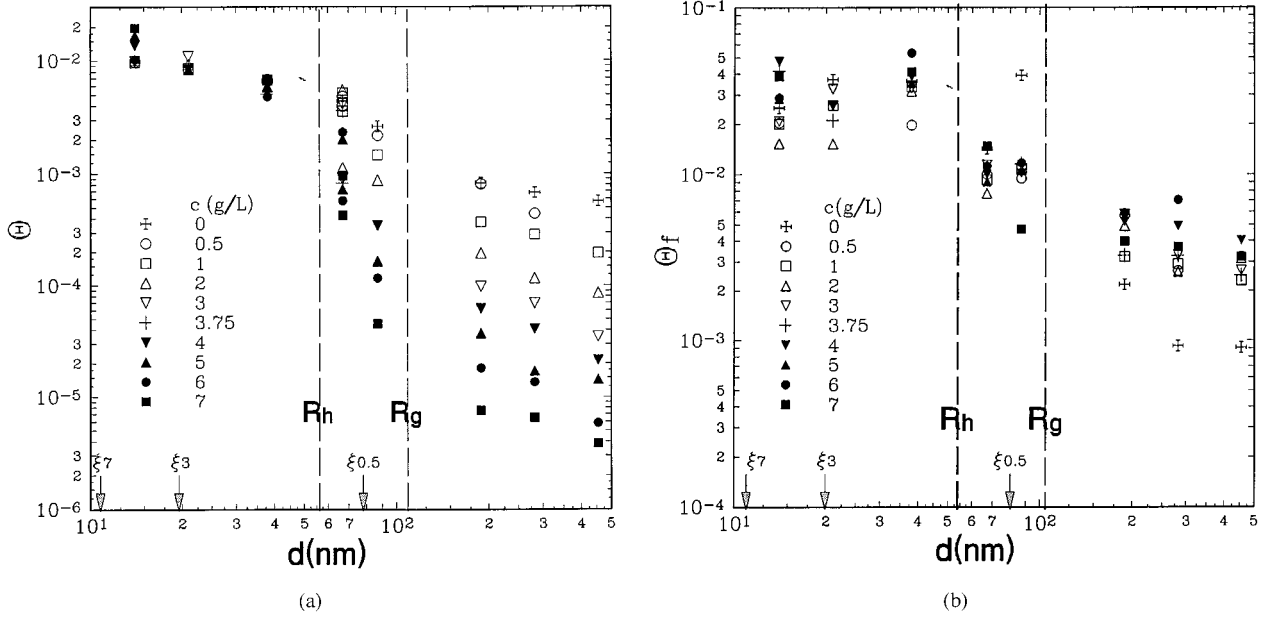
Figure 1. Probe diameter dependences of the relaxation pseudorates θ and θ_f [eq. (4)] at various indicated concentrations c for different modes of small and large probes in solutions of 1 MDa HPC: (a) θ for the slow mode; and (b) θ_f for the fast mode. Vertical dashed lines indicate the hydrodynamic radius R_h and the radius of gyration R_g of the polymer. Arrows indicate the mesh size ξ calculated as $R_g\left(\dfrac{c}{c^*}\right)^{-3/4}$, where c^* is an overlap concentration.

a net with a mesh size ξ, allowing small probes with radius $R < \xi$ to diffuse through the polymer net following the solvent flow, and effectively trapping large probes with $R > \xi$, forcing them to move with the macroscopic viscosity of the solution. However, these models define[26] ξ as R_g at the overlap concentration c^* and predict a strong concentration dependence of ξ in the form $\xi = R_g\left(\dfrac{c}{c^*}\right)^{-3/4}$. Therefore, according to the transient gel models, the separation length scale between small- and large-probe regimes should be a c-dependent mesh size ξ, which directly contradicts our finding that the transition length scale is independent of c. On the other hand, the transition region location at (R_h, R_g) and its independence from the polymer concentration is consistent with the fundamental importance of hydrodynamic interactions in probe diffusion.

A similar transition in probe behavior can be seen in Figure 1(b), which plots θ_f vs. d. Again, there are two probe regimes: (1) small ($d < R_h$) probes with a θ_f that is independent of d, and (2) large ($d > R_g$) probes with a θ_f that weakly decreases (within a factor of 2) with increasing d. In the transition regime $R_h < d < R_g$, as d is

increased from 40 to 180 nm, θ_f falls by a factor of 10. However, in both the large- and the small-probe regimes, θ_f is largely c independent.

Figure 2 gives the concentration dependence of θ and θ_f for probes of all sizes. As seen in Figure 2(a), for small probes, θ is largely concentration independent, while for large probes θ decreases with increasing c, closely following

$$\theta = \theta_o \exp(-\alpha c^\nu). \tag{5}$$

Here, α is a scaling prefactor, ν is a scaling exponent, and θ_0 is the intercept. Figure 2(b) shows the concentration dependence of θ_f. θ_f of both small and large probes is largely c independent (within factor of 2), just as θ of the small-probe slow mode was independent of c.

From the c dependence of θ, one can separate the slow modes of large and small probes from each other. For the fast mode, the c dependences of θ_f of small and large probes are very similar. However, the d dependence of θ_f [Fig. 1(b)] allows one to separate the small- and large-probe fast modes. The similarities in the concentration dependences of three out of four modes raises the
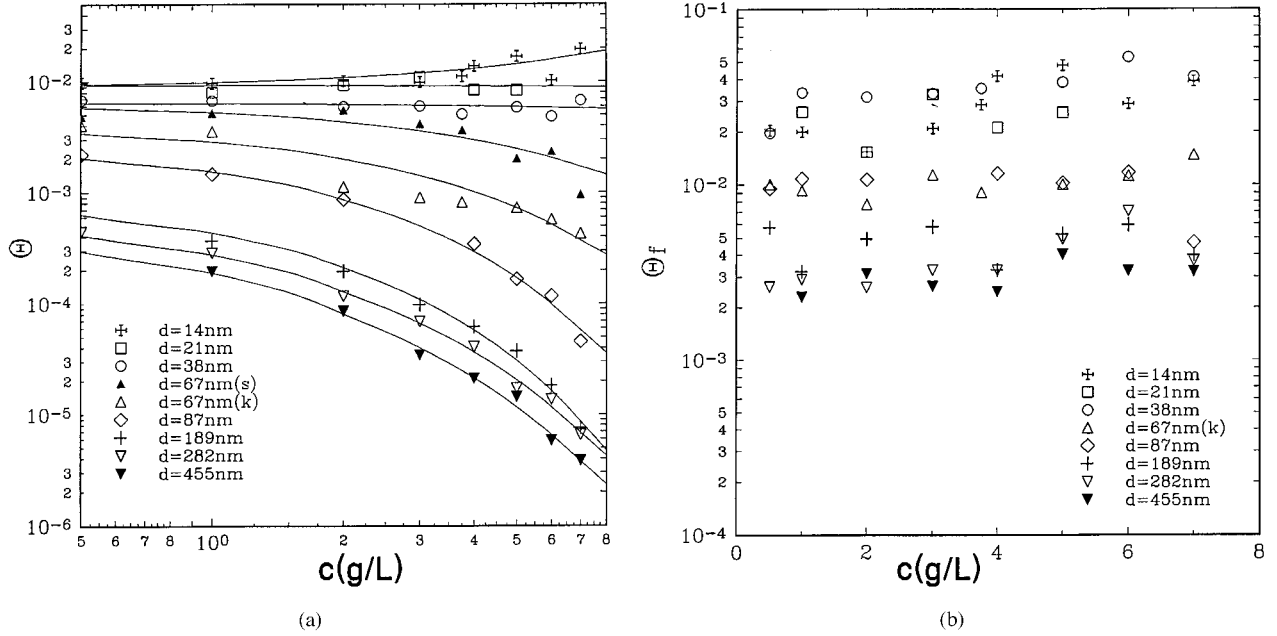
Figure 2. Concentration dependences of the relaxation pseudorates θ_f and θ_f [eq. (4)] for small ($d \leq 67$ nm) and large ($d \geq 67$ nm) probes in solutions of 1 MDa HPC: (a) θ of the slow mode; and (b) θ_f of the fast mode. Solid lines on Figure 2(a) are stretched exponentials in c. Units of θ are $(\mu S)^{-\beta}$.

question of the relation of the modes to each other. If one compares the absolute values of θ and θ_f for all three modes, one finds that the four modes have only three time scales, namely: (1) the large-probe slow mode with $\theta \sim 10^{-3}$–5 $\times 10^{-6}$, (2) the large-probe fast mode and the small-probe slow mode with θ_f or $\theta \sim 1 \times 10^{-2}$–3 $\times 10^{-3}$, and (3) the small-probe fast mode with $\theta_f \sim 5 \times 10^{-2}$.

Mode time scales may also be characterized by relaxation times $\tau = \theta^{-1/\beta}$ and $\tau_f = \theta_f^{-1/\beta_f}$. τ and τ_f have dimensions of (time),[1] so they are inequivalent to θ and θ_f, which have dimensions (time)$^{-\beta}$. For four mode/probe-size combinations, τ and τ_f are: (a) $\tau \sim 10^{-3}$–3 $\times 10^{-1}$ s for the large-probe slow mode, (b) $\tau_f \sim 6 \times 10^{-4}$–$10^{-1}$ s for the large-probe fast mode, (c) $\tau \sim 10^{-4}$–8 $\times 10^{-4}$ s for the small-probe slow mode, and (d) $\tau_f \sim 3 \times 10^{-4}$–5 $\times 10^{-2}$ s for the small-probe fast mode.

The longest time scale involves the large-probe slow mode, which has the largest τ. We can rationally incorporate the large-probe fast mode (τ_f^{large}) and the small-probe slow mode (τ^{small}) into a single intermediate time scale. The small-probe fast mode, while strongly scattered, usually satisfies $\tau_f^{\text{large}} \geq \tau_f^{\text{small}} \geq \tau^{\text{small}}$; for small probes $\tau_f > \tau$ even though $\theta_f > \theta$. This difference between

τ and θ arises because for small probes $\beta \approx$ 0.5–0.9 but $\beta_f \approx$ 0.2–0.5. It is legitimate to inquire whether we should interchange θ and θ_f for the small spheres; indeed, on a plot of $g^{(1)}(q, t)$ the visible decay of $\exp(-\theta t^\beta)$ occurs before the visible decay of $\exp(-\theta_f t^{\beta_f})$, because the relative values of β and β_f cause the slowest of the fast-mode components to decay at later times than the slowest slow mode component decay. However, as seen in Figures 1 and 2, θ and θ_f have smooth dependences on d and c. If one were to interchange θ and θ_f of the small spheres, Figures 1 and 2 would show that θ and θ_f each had nonmonotonic dependences on d and c. It is, therefore, rational to label the small-probe (θ_f, β_f)-mode as the "fast" process, even though $\tau_f^{\text{small}} \geq \tau^{\text{small}}$.

We now consider the physical properties of the modes, in terms of a three time scale description of the system:

Mode Concentration Dependences

First, we compare the concentration dependences of θ and θ_f with the concentration dependence of the zero-shear viscosity η. Figure 3 shows the c dependences of $\theta\eta$ [Fig. 3(a)] and $\theta_f\eta$ [Fig. 3(b)]. η
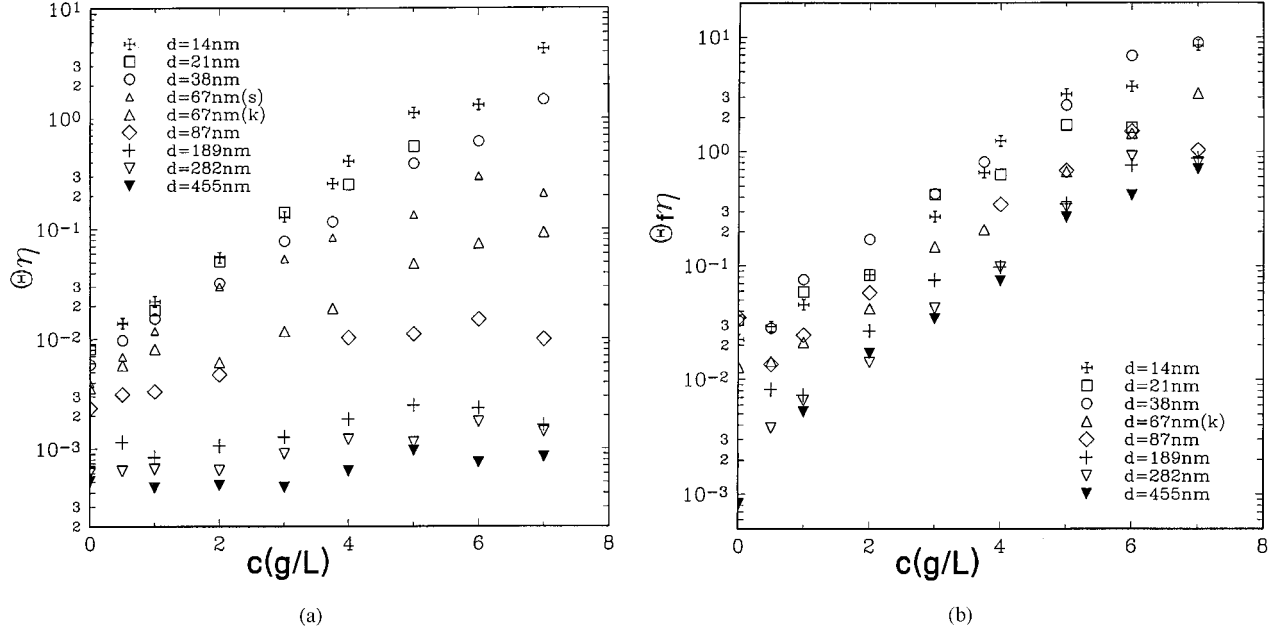
Figure 3. Concentration dependences of the product of the relaxation pseudorate and solution viscosity for small ($d \leq 67$ nm), and large ($d \geq 67$ nm) probes in solutions of 1 MDa HPC: (a) $\theta\eta$ of the slow mode; (b) $\theta_f\eta$ of the fast mode. θ and θ_f are from eq. (4). η is from ref. 27.

is from the viscosity measurements of Quinlan and Phillies.[27] Consider the slow mode [Fig. 3(a)]: (1) for small probes ($d \leq 67$ nm): θ does not track η^{-1} at all; $\theta\eta$ increases 20–400-fold as c increases from 0 to 7 g/L; (2) for the largest probes ($d = 189, 282, 455$ nm), $\theta\eta$ is a constant to within a factor of 2 of its average value. On the other hand, consider the fast mode [Fig. 3(b)]: for spheres of all sizes $\theta_f\eta$ increases 100- to 400-fold as c is increased from 0 to 7 g/L. Therefore, of the four mode/probe-size combinations only the slow mode of the large probes shows close compliance with Stokes–Einsteinian behavior ($\theta\eta \approx$ const). In other words, at long times the relaxation of probes that are larger than the chain dimensions follows the macroscopic viscosity η of the polymer solution. For the fast mode of large probes, and the slow and the fast modes of small spheres, probe motions at elevated polymer concentrations are much faster than motions that one would expect on the basis of the macroscopic solution viscosity.

Mode-Scattering Vector Dependences

Second, we consider the dependences of the fitting parameters on the scattering vector. Figure 4(a) shows the q dependence of θ for the slow mode of large probes. The relaxation rate θ clearly shows

diffusive behavior, i.e., $\theta \sim aq^2$; there is no intercept at $q = 0$. This diffusive behavior confirms our above suggestion on the origin of the large-probe slow mode, namely that the large-probe slow mode describes a time scale so long that polymer : solvent internal modes have completely relaxed. To the probes, on this time scale the medium is a simple viscous fluid. Therefore, from the central limit theorem one can predict that probes perform simple Brownian motion, implying $\beta_t = 1$ and $\theta \sim q^2$, as found experimentally.

Figure 4(b) shows the q dependence of the intermediate time scale mode, which incorporates the large-probe fast mode and the small-probe slow mode. The slow mode of small probes shows[20] a clear diffusive behavior with $\theta \sim aq^2$ and zero intercept as $q \rightarrow 0$. However, the fast mode of large probes has a very complicated q behavior. As seen in Figure 4(b), θ_f of large probes is largely independent of q at small angles ($q < 250$ μm^{-2}), but has a linear dependence $\theta_f \sim aq^2 + b$ with nonzero intercept b at large angles ($q > 250$ μm^{-2}).

Finally, the q dependence of the short time scale mode (the fast mode of small probes) is complex,[20] having two linear regimes, namely θ_f
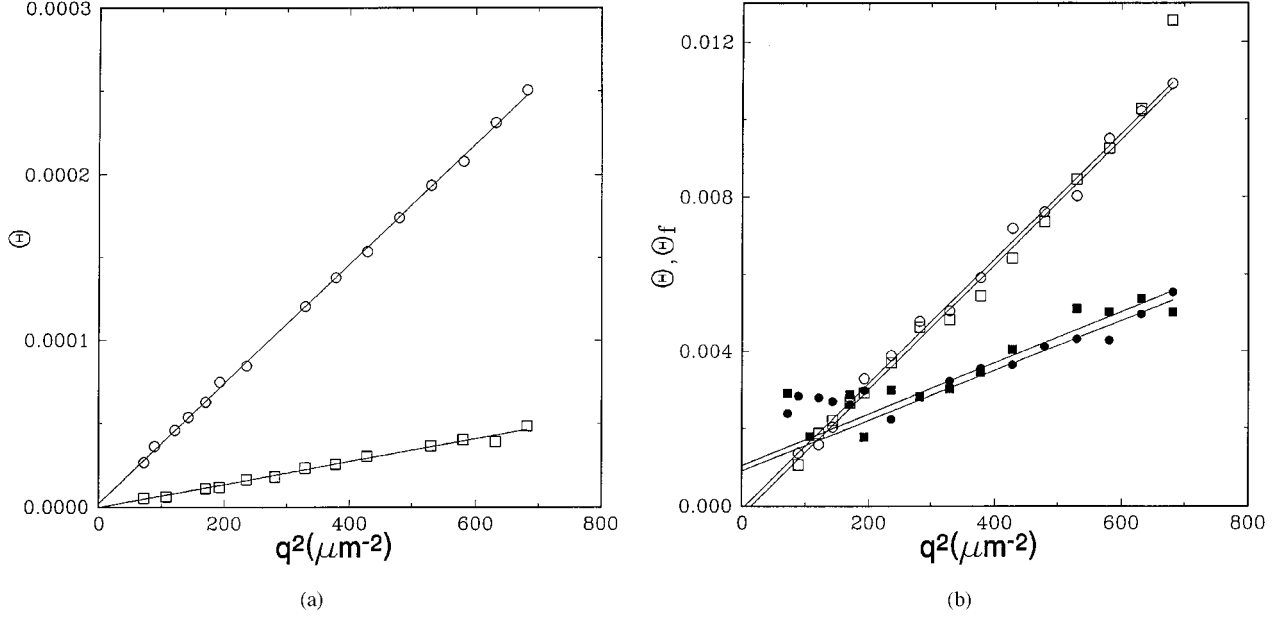
Figure 4. q-Dependence of the relaxation pseudorates for probes in HPC : water in different time scale regimes: (a) long time scale θ of large 189 nm probes in 2 g/L ($\bigcirc$), and 5 g/L ($\square$) HPC; (b) intermediate time scale θ of small 21 nm probes in 1 g/L ($\bigcirc$), 4 g/L ($\square$) HPC, and θ_f of large 189 nm probes in 2 g/L ($\bullet$), 5 g/L ( ) HPC. Solid lines are best linear fits. Point ($\boxtimes$) on (b) was omitted from the fit.

$\approx a q^2$ at large q and $\theta_f \approx a_1 q^2 + b$ with $b \neq 0$ at small q.

The fraction of the fast mode A_f depends differently on q for small and large probes. Figure 5 shows q dependences of A_f for large and small probes. For large probes, A_f at small q increases weakly with rising q, but is independent of q at large q. The crossover in $A_f(q)$ between small- and large-q behavior happens at the same q as the crossover in $\theta(q)$ for large probes. The crossover is at $q^2 \approx 250\ \mu m^{-2}$, equivalent to a crossover distance $q^{-1} \approx 63$ nm, 63 nm also being the distance scale on which small- and large-probe behaviors cross over. On the other hand, for small probes, A_f decreases quasi-exponentially with increasing q; if one identifies the large-probe fast mode with the small-probe slow mode, the amplitude of this mode has similar q dependence for large and small probes.

Mode-Stretching Exponents

Third, we consider the stretching exponents of three time scale regimes. The long time scale regime (large-probe slow mode) has[20] $\beta = 1$. The intermediate time scale regime (large-probe fast and small-probe slow) have[20] β and β_f in the same range (0.6, 0.95). β of small probes and β_f of large probes both monotonically decrease[20] with increasing c from 0.95 near $c = 0$ to 0.6 at 7 g/L HPC. Also, β of small probes and β_f of large probes are both q independent,[20] even though $A_f(q)$ and $\theta_f(q)$ are very different for the small-probe slow and large-probe fast modes. The short time scale regime (the small-probe fast mode) has[20] the smallest stretching exponent; $\beta_f \in$ (0.2, 0.6). β_f of small probes also decreases[20] with increasing c, but has a nontrivial q dependence (at low q, β_f decreases with increasing q, at high q, β_f is q independent).

The aforementioned properties demonstrate that modes on the three time scales in general differ from each other. Physical interpretations for the intermediate and short time scale regimes will be advanced in the following sections. Here we will distinguish the properties of these two time scale modes and identify justifications, in addition to the similar time scale, for combining the large-probe fast mode and the small-probe slow mode into a single intermediate time scale regime.

First, consider the intermediate time scale regime. Two modes (the large-probe fast- and small-probe slow-modes) compose the intermediate time
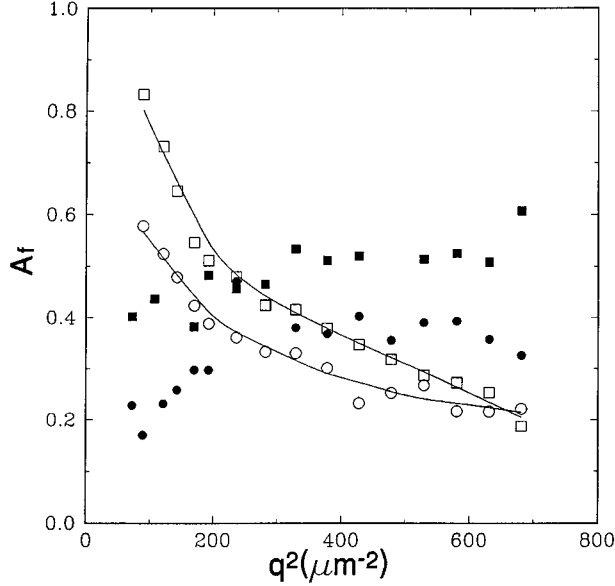
Figure 5. Amplitude fraction parameter A_f of the fast mode from eq. (4) as a function of q^2 for 21-nm probes in 1 g/L (○) and 4 g/L (□) HPC, and for 189-nm probes in 2 g/L (●) and 5 g/L ( ) HPC. Lines are drawn to guide the eye.

increase with rising c. The decay pseudorates θ and θ_f are concentration independent; τ and τ_f inherit their dependences on c exclusively from β and β_f.

Second, consider the short time scale regime, i.e., the small-probe fast mode. Several properties of this mode distinguish it from others. In addition to having the largest relaxation pseudorate θ_f, this mode has the smallest stretching exponent β_f. This combination of large θ_f and small β_f makes this mode very broad, so that $\tau_f > \tau$ with a very sharp initial decay. Other properties of this mode appear to be similar to properties of the intermediate time scale mode. In particular, the short time scale mode shows non-Stokes–Einsteinian behavior; to first approximation, θ_f is c independent. The stretching exponent β_f of the short time scale regime decreases with increasing c, just as the stretching exponents of the intermediate time scale mode do. However, the relaxation time τ_f of the short time scale regime appears to be c independent, in contrast to the c dependence of τ and τ_f of the intermediate time scale mode.

Summarizing, we have analyzed the properties of the four mode/probe-size combinations and have identified three physical time scales of probe motion. The large-probe slow mode corresponds to the longest time scale. The properties of this mode

scale. The large-probe fast and the small-probe slow modes differ significantly only in their q dependences. This difference in q dependence can be rationalized as the effect of probe size on the coupling of probe motions to the chain relaxations. In all other physical properties revealed by our previous study[20] these two modes are similar. Particular similarities between the large-probe fast mode and the small-probe slow mode include: (1) stretched-exponential (not simple-exponential) observed spectral lineshapes; (2) c independences of θ for small probes and θ_f for large probes (within a factor of 2); (3) noncompliance of mode pseudorates with a Stokes–Einstein equation (large probes: $\theta_f \eta \neq$ const; small probes: $\theta \eta \neq$ const); (4) very weak (large probes) or no (small probes) d dependence of θ_f or θ, respectively, and (5) β_f (large probes) and β (small probes) both fall with increasing c from 0.95 in pure solvent to 0.6 at 7 g/L of polymer.

Figure 6 compares τ of small probes and τ_f of large probes. Solid lines are drawn through the data on small probes (τ) to guide the eye and to help distinguish τ of small probes from τ_f of large probes. If the c dependences of θ (and β) and θ_f (and β_f) are the same for these two modes, then the c dependences of the true relaxation rates τ and τ_f should be the same. τ and τ_f indeed both
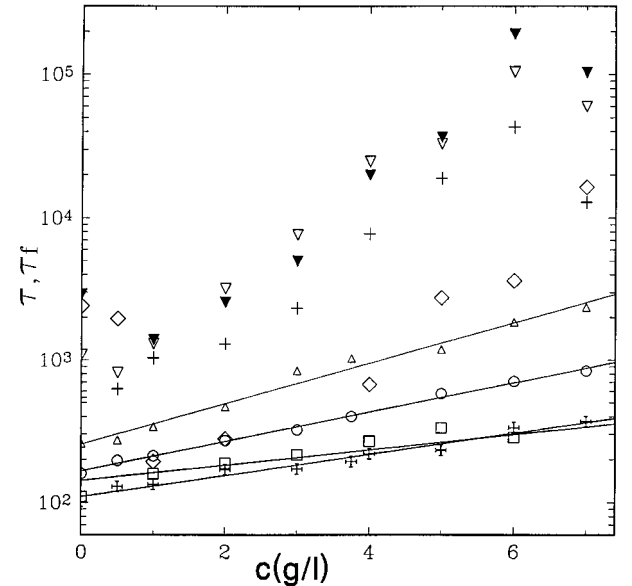

Figure 6. Concentration dependences of relaxation times: $\tau = \theta^{-1/\beta}$ for the slow mode of small probes with diameter 87 (◇), 189 (+), 282 (▽), and 455 (▼) nm. Units of τ and τ_f are (μS). Solid lines are drawn to guide the eye through the data on small probes (τ).

indicate that on this time scale the polymer solution behaves as a simple viscous fluid, and spheres sample the macroscopic viscosity of the solution. The intermediate time scale incorporates the small-probe slow mode and large-probe fast mode. These two modes have similar physical properties, except for their q dependences, differences which can be attributed to a probe-size effect. The small-probe fast mode corresponds to the shortest time scale. Most properties of this mode are very different from other modes, except for a few properties that are similar to the intermediate time scale regime, notably the non-Stokes–Einsteinian behavior and, to first approximation, some but not all q dependences.

COUPLING/SCALING ANALYSIS

The coupling model of Ngai[28–32] is a general model for "the dynamics of constrained, interacting systems."[21] The coupling model has been successfully applied to a variety of complex physical systems.[32] Even though the coupling model for real complex systems has no theoretical derivation from the first principles yet, from simulating simple systems with idealized Hamiltonians there are several encouraging theoretical results[33–35] that directly support basic elements of the coupling model. The most recent examples of such theoretical modeling via computer dynamics simulations are (1) the relaxation of interacting arrays of coupled nonlinear oscillators,[34] and (2) the Fermi acceleration problem with added nonlinearity.[35] In both theoretical examples, the basic principles of classical mechanics were used to estimate the effects of nonlinearity on the relaxational processes. Both simulations yielded the coupling model predictions for nonlinearly coupled many-body systems.

The coupling model looks at a system as a combination of "basic units" interacting nonlinearly with each other. The simple coupling model considers two time scales, separated by a crossover time t_c. At $t < t_c$, "basic units" are assumed to relax independently from each other; their relaxation can be described by a correlation function

$$\phi(t) = \exp(-t/\tau_0), \qquad t < t_c. \quad (6)$$

τ_0 is the characteristic time for unconstrained relaxation. At $t > t_c$, cooperative constrains between "basic units" become important, and the degree n ($0 \leq n < 1$) of coupling between basic units should be accounted for in $\phi(t)$, so that

$$\phi(t) = \exp(-(t/\tau)^{(1-n)}), \qquad t > t_c. \quad (7)$$

Here, τ is the characteristic time for relaxations under constrains. There is also a continuity condition on $\phi(t)$ at $t = t_c$, which yields the requirement $\tau = [t_c^{-n}\tau_0]^{1/1-n}$. The coupling model is not specific on which interactions (e.g., hydrodynamic, topological) create the cooperative constraints.

The coupling model successfully predicts some experimental results on probe diffusion in polymer solutions[11,15,17] and on polymer self-diffusion.[36–38] First, stretched-exponential functions of $\phi(t)$ describe well $g^{(1)}(t)$ of many polymer systems.[11,15,17,39–41] In terms of our notation, $\beta = 1 - n$. Second, it was shown by Ngai and Phillies[21] that the phenomenological concentration dependence of β[11,15,17,40,42] is often consistent with coupling model predictions for $1 - n$. Third, the coupling model predicts[21] that the relaxation time τ depends on q as $\tau \equiv \theta^{-1/\beta_q} \sim q^{-2/(1-n)}$. This q dependence was seen experimentally[15] in our laboratory.

Recently, Ngai and Phillies[21] advanced coupling/scaling arguments providing one with an additional two ways to extract the degree of coupling n from the phenomenology. The first way is the use of the concentration dependence of the probe diffusion coefficient D_s, where coupling/scaling gives the degree of coupling n_D, namely

$$\beta_c \equiv 1 - \eta_D$$

$$= \left[\frac{3\nu}{2} + \frac{(3\nu - 1)(\ln(D_s(c^*)) - \ln(D_s(c)))}{2 \ln(c/c^*)} \right]^{-1}. \quad (8)$$

Here, c^* is a nominal overlap concentration, and ν from $R_g \sim M^\nu$ relates the radius of gyration R_g of a polymer to its molecular weight M. Equation (8) is most plausible for nondilute solutions, i.e., for $c \geq 2c^*$.

The second way is the use of the concentration dependence of η, where coupling/scaling gives the degree of coupling n_η, namely

$$\beta_\eta \equiv 1 - n_\eta$$

$$= \left[\frac{3\nu}{2} + \frac{(3\nu - 1)(\ln(\eta(c)) - \ln(\eta(c^*)))}{2 \ln(c/c^*)} \right]^{-1}. \quad (9)$$

Equations (8) and (9) provide two paths for obtaining the degree of coupling $n \equiv 1 - \beta$. Two additional independent ways for obtaining the degree of coupling are: (1) β_t from the t dependence of $g^{(1)}(t)$, and (2) β_q from the q dependence of $g^{(1)}(t)$. An obvious way to test the coupling/scaling model is to compare β_t, β_q, β_c, and β_η for experimental data on one system. If all four β agree with each other, then the model is self-consistent. Phillies and Ngai[21] were able to demonstrate the success of the model for probe diffusion[17] in 300 kDa HPC solutions. They demonstrated that β_c, β_q, and β_t from $g^{(1)}(t)$, and β_η from $\eta(c)$ agree with each other.

Recently, we[22] applied the coupling/scaling model to the data of ref. 20 on $M = 1 \times 10^6$ Da HPC. A simple repeat of the coupling/scaling analysis was impossible, because the spectra of ref. 20 have two relaxational modes, not one. Ref. 20's spectra do not imply a single diffusion coefficient D_p that could be substituted in eq. (8). The two modes appear to be very different in their physical nature. In particular, large probe diffusion requires whole-chain center-of-mass motions, but small probe diffusion can be accommodated by local chain motions. As shown in the previous section, the slow mode of large probes reflects a simple Brownian motion of the probes in the polymer matrix; regarding other modes, ref. 22 proposed that the intermediate time scale mode involves probe motions coupled to chain local motions.

Because the spectral lineshape is bimodal, we cannot apply the simple coupling/scaling model[21] to the whole relaxation. However, very recently Ngai and Rendell[43] have shown an approach to applying the coupling model to a much more complicated relaxation, namely diffusion in a concentrated solution of hard colloidal spheres as studied by Segre and Pusey.[44] In these systems, the light-scattering spectrum is composed of a short-time pure exponential regime, an intermediate-time stretched exponential-in-time regime, and a long-time pure exponential regime. Ngai and Rendell[43] concluded that the coupling model procedures are applicable to this systems, in that "there is good agreement between [the model] and experiment."

In contrast to the system described by Ngai and Rendell,[43] in which the functional form of the relaxation depends on time, so that three time regimes exist, here we have bimodal spectra that are represented as a sum of two independent modes. The coupling ansatz naturally leads to such spectra if the system contains several groups of fundamental units that are strongly coupled within each group, but that are very weakly coupled between groups. We,[22] therefore, analyzed each mode separately using coupling/scaling, so as to determine which modes are described by the coupling model.

Two sets of coupling coefficients, namely β_t and β_c for the slow mode, and β_{ft} and β_{fc} for the fast mode, were obtained[22] from the measured $g^{(1)}(t)$ and eq. (8). β_{eta} is calculated using eq. (9) from $\eta(c)$, so β_η is the same for all modes. Dealing separately with each mode, we can compare β_t, β_c, β_{ft}, and β_{fc} to β_η to infer the coupling behavior of each mode. β_η is very important in these comparisons because it reflects the motion of complete chains (a matrix property unrelated to probe radius), and because it is calculated directly from coupling/scaling analysis[21] without auxiliary assumptions.

We found[22] that some modes follow the coupling/scaling model, while others do not. The slow mode of large probes and the fast mode of small probes do not follow coupling/scaling predictions, so these modes are not considered further here. The intermediate time scale regime (small-probe slow mode and large-probe fast mode) obeys the coupling/scaling model. We consider here this time scale mode in detail.

Figures 7(a) (small-probe slow mode) and 7(b) (large-probe fast mode) show exemplary results of the coupling/scaling analysis for the small-probe slow mode and the large-probe fast mode, respectively, comparing β_t and β_c (or β_{fc}) with β_η from the solution viscosity. To apply eqs. (8)–(9), one needs a nominal overlap concentration c^* and scaling exponent ν. From ref. 27, for 1 MDa HPC $c^* = 1/[\eta]$ is 1.4 g/L. We tried three plausible values for ν, namely 0.5, 0.55, and 0.6. The β_η and β_c calculated with a specific ν are denoted $\beta_{\eta,\nu}$ and $\beta_{c,\nu}$, respectively. Near c^*, $\beta_{\eta,\nu}$ is scattered because of a numerical artifact; at c^*, eq. (9) approaches $\ln(1)/\ln(1)$. For $c > c^*$, $\beta_{\eta,\nu}$ decreases smoothly with increasing c.

From Figure 7(a), the small-probe slow mode has $\beta_t \approx \beta_{c,0.55}$ at $c > 3$–4 g/L, which is in agreement with the coupling/scaling model. Furthermore, at $c > 3$–4 g/L, $\beta_t \approx \beta_{\eta,0.5}$. The concentration threshold of 3–4 g/L, above which the model applies, is more than twice c^*. The fact that $\beta_t \approx \beta_{c,0.55}$ is true only at $c > 2c^*$, is consistent with expectations of ref. 21 that coupling/scaling is more likely to be valid in a nondilute solution. The finding $\beta_t \approx \beta_{c,0.55} \geq \beta_{\eta,0.55}$
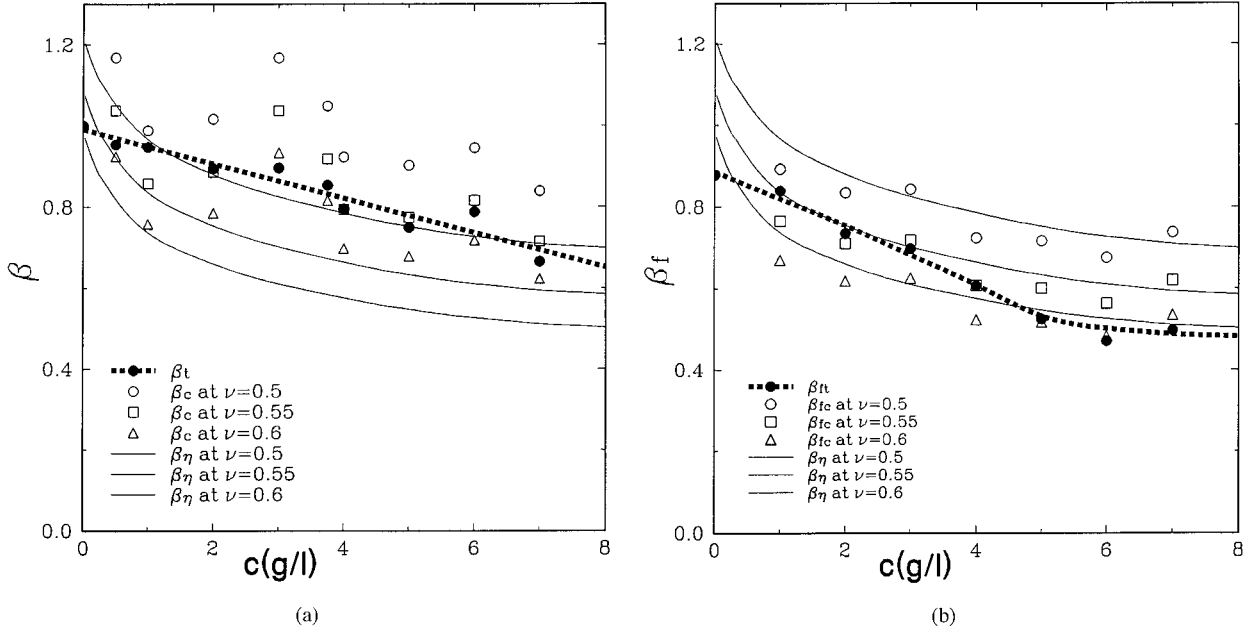
Figure 7. Concentration dependences of the stretching exponents for the intermediate time scale regime: (a) the small-probe (14 nm) slow-mode exponents β_t from $g^{(1)}(t)$ via eq. (4), and β_c from θ via eq. (8) (for three values of ν); and (b) the large-probe (455 nm) fast-mode exponents β_{ft} from $g^{(1)}(t)$, and β_{fc} from θ_f (for three values of ν). Parts (a) and (b) also show β_η from η^{27} via eq. (9) (solid lines corresponding, top to bottom, to 0.5, 0.55, and 0.6. Dashed lines, drawn to guide the eye, correspond to $\beta_c(c)$ and $\beta_{fc}(c)$.

is not exactly the result one would expect from a self-consistent model.[21] However, the inequality between β_η and β_t at $c > 2c^*$ for small probes is consistent with coupling/scaling predictions. β_η describes relaxations of whole chains; β_t and β_c describe probe motions. Under the coupling model,[21] the strength of dynamic constraints is reflected in the degree of coupling n. Because viscous flow moves whole chains, while small probes with $d \leq R_g$ can diffuse while displacing only part of the neighboring chain, polymer chain motions encounter larger dynamic constraints than probe motions, implying $\beta_t \approx \beta_c > \beta_\eta$, as found experimentally. Therefore, Figure 7(a) largely supports the coupling/scaling model predictions. Figure 7(b) shows that for the large-probe fast mode $\beta_t \approx \beta_{c,0.6} \approx \beta_{\eta,0.6}$, in the excellent agreement with the coupling/scaling model.

DISCUSSION

Ref. 20 found four relaxation modes in optical probe diffusion spectra. We have argued here that these four modes can be rationally divided into three physical regimes: (1) a long time scale re-

gime; (2) an intermediate time scale regime; and (3) a short time scale regime. The rationale for dividing these modes into three regimes is based on their physical properties, notably the time scale of the mode relaxation (the four modes decay on only three different time scales), and the value of the stretching parameters β and β_f [only three regimes: $\beta = 1$, β, $\beta_f \in (0.6, 1)$, and β, $\beta_f \in (0.2, 0.6)$]. Table I summarizes these differences.

What is the physics underlying the time scale regimes? We know the physical nature of the longest time scale regime. As noted above, the large-probe slow mode describes the motion of probes on time scale so long that the solution acts as a sample viscous liquid. Correspondingly, large probes perform Brownian motion with $\theta \sim q^2$, $\beta = 1$ and follow the Stokes–Einstein equation ($\theta\eta \approx$ const).

Now we consider the properties of other two regimes. We start with the two modes of the intermediate time scale regime. As mentioned in previous sections, the small-probe slow mode and the large-probe fast mode have common properties, except for their q dependences. This difference in q dependences can be rationalized as the

Table I. Properties of the Four Relaxational Modes for Large and Small Probe Diffusion in 1 MDa HPC

	Mode	
Probe Size	Slow	Fast
Large probes $(d > R_g)$	$\theta \sim 10^{-3} - 5 \times 10^{-6}$ $\beta = 1$ $\theta \sim \exp(-\alpha c^{\nu})$ $\theta \sim a q^2$ $\theta \downarrow$ with $d \uparrow$, $\alpha \sim d$ $\dfrac{\theta \eta}{\theta_0 \eta_0} \approx$ const (within 2)	$\theta_f \sim 10^{-2} - 3 \times 10^{-3}$ $\beta_f \in (0.6, 0.95)$ $\theta_f \sim c^0$ (within 2) $\theta_f(q^2)$—complicated $\theta_f \sim d^0$ (within 2) $\dfrac{\theta_f \eta}{\theta_{f0} \eta_0} \neq$ const $\beta_f \downarrow$ with $c \uparrow$ $\beta_f \sim q^0$
Coupling/scaling (c/s) analysis	A_f largely independent of q $\dfrac{d\tau}{dc} > 0$ $1 \equiv \beta_t > \beta_{c,\nu} \approx \beta_{\eta,\nu}$ c/s fails	A_f largely independent of q $\dfrac{d\tau_f}{dc} > 0$ $\beta_{ft} \approx \beta_{fc,\nu} \approx \beta_{\eta,\nu}$ c/s successful
Small probes $(d < R_g)$	$\theta \sim 10^{-2} - 3 \times 10^{-3}$ $\beta \in (0.6, 0.95)$ $\theta \sim c^0$ $\theta_f \sim q^2$ $\theta_f \sim d^0$ (within 2) $\dfrac{\theta \eta}{\theta_0 \eta_0} \neq$ const $\beta \downarrow$ with $c \uparrow$ $\beta \sim q^0$ $A_f(q)$—very strong $\dfrac{d\tau}{dc} > 0$	$\theta_f \sim 5 \times 10^{-2}$ $\beta_f \in (0.2, 0.6)$ $\theta_f \sim c^0$ (within 2) $\theta_f(q)$—complicated $\theta_f \sim d^0$ $\dfrac{\theta_f \eta}{\theta_{f0} \eta_0} \neq$ const $\beta_f \downarrow$ with $c \uparrow$ $\beta \sim q^0$ $A_f(q)$—very strong $\tau_f \sim c^0$
Coupling/scaling (c/s) analysis	$\beta_t \approx \beta_{c,0.55} \geq \beta_{\eta,0.55}$ c/s largely successful	$\beta_{ft} \leq \beta_{\eta,\nu} \leq \beta_{fc,\nu}$ c/s fails

All notation defined in text.

effect of probe size on the coupling of probe motions to polymer relaxations. On this time scale, large probes are fully coupled to polymer solution motions at all but very long distances (low q), because at long distances probes have a chance to decouple from chain internal motions and experience the long wavelength shear viscosity. Correspondingly, A_f is independent of q at all but very low q. However, the q dependence is very marginal: A_f is independent of q over 85–90% of the studied q scale. Small probes are small enough ($d < 2R_g$) to be sensitive to the solution structure, in addition to sensing the shear viscosity of the medium. As a result, the spatial dimensions of the chain become important to the probe and A_f (as well as θ_f) show a strong dependence on q.

The above-mentioned q dependence differences between the two modes of the intermediate time scale regime can, therefore, be rationalized in terms of the probe coupling to the polymer. The two modes of the intermediate time scale regime also have the common properties, mentioned in the Results section. Can these properties also be rationalized in terms of the probe motions coupled to polymer relaxations?

Experimental phenomenology supportive of an interpretation of intermediate mode properties as arising from motions of probes coupled to polymer motions includes: (a) the observed lineshape is a stretched exponential, not a simple exponential in t; (b) β (small spheres) and β_f (large spheres) fall with increasing c, consistent with the coupling

model expectation that the coupling coefficient n = 1 − β increases with increasing c, because the coupling of probes to polymers is stronger at higher polymer concentrations; and (c) both modes of the intermediate time scale largely comply with the coupling/scaling prediction β_t = β_c = β_η, namely for large spheres $\beta_{ft} \approx \beta_{fc,\nu} \approx \beta_{\eta,\nu}$, while for small spheres $\beta_t \approx \beta_{c,\nu}$, (though β_t, $\beta_{c,\nu} \geq \beta_{\eta,\nu}$). The above three properties were directly predicted by the coupling/ scaling model.[21] Other phenomenological findings that are consistent with the idea that the intermediate time scale mode reflects the motion of probes, coupled to polymer relaxations, include: (1) θ (small spheres) and θ_f (large spheres) are practically independent of d (within a factor of 2). A mode whose dynamics is largely determined by chain motion, in which probes are passive witnesses to the chain–chain relaxations, could have a relaxation rate independent of d; (2) the q dependence depends on the probe size, as explained above; (3) neither θ nor θ_f tracks η^{-1}. The relaxation pseudorates of the two modes do not simply reflect the macroscopic viscosity of the solution, because probes, in addition of being sensitive to long wavelength shear viscosity, also are coupled to polymer relaxations; (4) τ (small probes) and τ_f (large probes) depend on c. A mode with a strong coupling to polymer relaxations should have a concentration-dependent relaxation rate, because at higher c dynamic constraints are stronger, so the relaxations are slower; and (5) the concentration dependence of the large-probe τ_f is stronger than the concentration dependence of the small-probe τ, consistent with the expectation that larger probes couple more strongly to polymer motions than do smaller probes.

We finish our mode analysis by considering the small-probe fast mode. We propose that at very short times probes sample local chain relaxations. The short time scale is sampled by the fast mode of small probes. These probes are much smaller than chains, so at our concentration a single small probe is unlikely to be in contact with more than one or two chains at a time. At short distances and times, chain interactions have not yet fully established themselves, so θ_f should be relatively independent of c, as observed experimentally. If probe motions are dominated by the motions of one neighboring chain, θ_f will be determined by internal chain dynamics of a single chain, and will be relatively independent of d, also as observed experimentally.

In summary, the four observed relaxation modes in optical probe diffusion spectra were shown to comprise three physical time scale regimes: (1) a long time scale regime, consisting of the large-probe slow mode; (2) an intermediate time scale regime incorporating the small-probe slow mode and the large-probe fast mode; and (3) a short time scale regime represented by the small-probe fast mode.

The proposed physical picture underlying these time scale regimes is based on the assumption that probe relaxations reflect motions of polymer chains that occur on the three physical time scales. On the longest time scale, all polymer modes have decayed and the solution behaves like a viscous fluid. In this time scale, probes sample the viscous fluid. The coupling/scaling model does not work for this regime. On the intermediate time scale, we propose that probe motions are coupled to polymer relaxations. The coupling/scaling model largely succeeds in describing this regime. The shortest time scale is not described by the coupling/scaling model. We propose that on this time and distance scale local motions of single chains are significant, and that probes sample local chain relaxations of individual chains.

REFERENCES

1. T. P. Lodge, N. Rotstein, and S. Prager, *Adv. Chem. Phys.,* **79,** 1 (1991).
2. D. N. Turner and F. R. Hallett, *Biochem. Biophys. A,* **451,** 305 (1976).
3. T.-H. Lin and G. D. J. Phillies, *J. Phys. Chem.,* **86,** 4073 (1982).
4. T.-H. Lin and G. D. J. Phillies, *J. Colloid Interface Sci.,* **100,** 82 (1984).
5. T.-H. Lin and G. D. J. Phillies, *Macromolecules,* **17,** 1686 (1984).
6. G. S. Ullmann and G. D. J. Phillies, *Macromolecules,* **16,** 1947 (1983).
7. L. M. Wheeler and T. P. Lodge, *Macromolecules,* **22,** 3399 (1989).
8. J. Won, C. Onyenemezu, W. G. Miller, and T. P. Lodge, *Macromolecules,* **27,** 7389 (1994).
9. L. M. Wheeler and T. P. Lodge, *Macromolecules,* **19,** 2983 (1986).
10. R. Furukawa, J. L. Arauz-Lara, and B. R. Ware, *Macromolecules,* **24,** 599 (1991).
11. G. D. J. Phillies, G. S. Ullmann, K. Ullmann, and T.-H. Lin, *J. Chem. Phys.,* **82,** 5242 (1985).

12. M. B. Mustafa and P. S. Russo, *J. Colloid Interface Sci.,* **129,** 240 (1989).
13. Z.-Bu and P. S. Russo, *Macromolecules,* **27,** 1187 (1994).
14. W. Brown and R. Rymden, *Macromolecules,* **19,** 2942 (1986).
15. G. D. J. Phillies, C. Richardson, C. A. Quinlan, and S.-Z. Ren, *Macromolecules,* **26,** 6849 (1993).
16. G. D. J. Phillies and D. Clomenil, *Macromolecules,* **26,** 167 (1993).
17. G. D. J. Phillies and M. Lacroix, *J. Phys. Chem. B,* **101,** 39 (1997).
18. G. D. J. Phillies, *J. Chem. Phys.,* **60,** 983 (1974).
19. G. D. J. Phillies, *Biopolymers,* **14,** 499 (1975).
20. K. A. Streletzky and G. D. J. Phillies, *J. Chem. Phys.,* **108,** 2975 (1998).
21. K. L. Ngai and G. D. J. Phillies, *J. Chem. Phys.,* **105,** 8385 (1996).
22. K. A. Streletzky and G. D. J. Phillies, *Coupling Analysis of Probe Diffusion in High Molecular Weight Hydroxypropylcellulose,* submitted.
23. G. D. J. Phillies, *J. Phys. Chem.,* **96,** 10061 (1992).
24. J. H. Noggle, *Physical Chemistry on a Microcomputer,* Little, Brown and Company, Toronto, 1985.
25. M. Doi and S. F. Edwards, *The Theory of Polymer Dynamics,* Oxford University Press, Oxford, 1986.
26. P.-G. de Gennes, *Scaling Concepts in Polymer Physics,* Cornell University Press, Ithaca, NY, 1979.
27. G. D. J. Phillies and C. A. Quinlan, *Macromolecules,* **28,** 160 (1995).
28. K. L. Ngai, A. K. Rajagopal, and S. Teiler, *J. Chem. Phys.,* **88,** 5086 (1988).
29. K. L. Ngai and R. W. Rendell, *J. Molecular Liquids,* **56,** 199 (1993).
30. K. L. Ngai, R. W. Rendell, A. K. Rajagopal, and S. Teiler, *Ann. NY Acad. Sci.,* **484,** 150 (1985).
31. A. K. Rizos, T. Jian, and K. L. Ngai, *Macromolecules,* **28,** 517 (1995).
32. K. L. Ngai, in *Disorder Effects in Relaxational Processes,* edited by R. Richert and A. Blumen, Springer, Berlin, 1994, pp. 89–150.
33. K. Y. Tsang and K. L. Ngai, *Macromol. Chem. Macromol. Symp.,* **90,** 95 (1995).
34. K. Y. Tsang and K. L. Ngai, *Phys. Rev. E,* **54,** R3067 (1996).
35. K. Y. Tsang and K. L. Ngai, *Phys. Rev. E,* **56,** R17 (1997).
36. J. Colmenero, A. Arbe, and A. Alegria, *Phys. Rev. Lett.,* **71,** 2603 (1993).
37. H. Walderhaug, B. Nystrom, F. K. Hansen, and B. Lindman, *J. Phys. Chem.,* **99,** 4672 (1995).
38. B. Nystrom, H. Walderhaug, and F. K. Hansen, *J. Phys. Chem.,* **97,** 7743 (1993).
39. B. Nystrom, J. Roots, A. Carlsson, and B. Lindman, *Polymer,* **33,** 2875 (1992).
40. B. Nystrom, K. Thuresson, and B. Lindman, *Langmuir,* **11,** 1994 (1995).
41. W. Brown and T. Nicolai, *Macromolecules,* **27,** 2470 (1994).
42. B. Nystrom and B. Lindman, *Macromolecules,* **28,** 967 (1995).
43. K. L. Ngai and R. W. Rendell, *Philos. Mag. B,* **77,** 621 (1998).
44. P. N. Segre and P. N. Pusey, *Phys. Rev. Lett.,* **77,** 771 (1996).